Electronic Supplementary Material (ESI) for Journal of Materials Chemistry A.

Nano-structured hybrid Molybdenum Carbides / Nitrides generated *in-situ* for HER Applications

Rajinder Kumar†[a] , Ritu Rai†[a], Seema Goutam[a], Abir De Sarkar[a], Nidhi Tiwari, Shambhu Nath Jha, Dibyendu Bhattacharyya[c], Ashok K Ganguli[ab]* and Vivek Bagchi[a]*

Supporting Information

List of Contents

S.1. Detailed information on synthesis of the catalysts

S.1.1. Synthesis of g-C_3N_4

Graphitic nitride was synthesized from reported method [1].

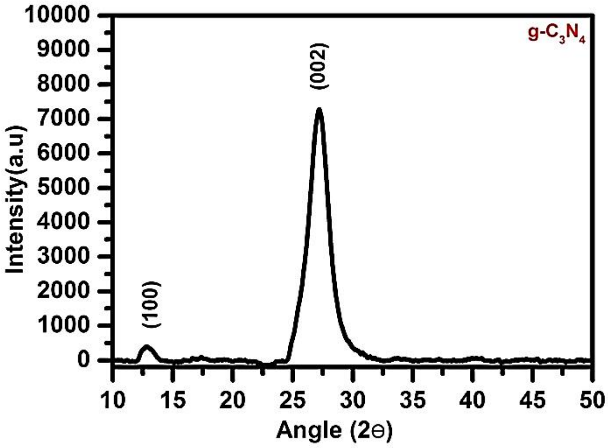

Fig S1.1: PXRD pattern of C_3N_4

S.1.2 Synthesis of Mo_2C and Mo_2N [2]

Carbon supported Mo_2C was synthesized by annealing the mixture of the metal precursor and graphitic carbon nitride in argon purged tubular furnace at 700 °C for two hours and similarly carbon supported Mo_2N was synthesized by annealing at 600 for 2 hours in NH_3 gas flow.

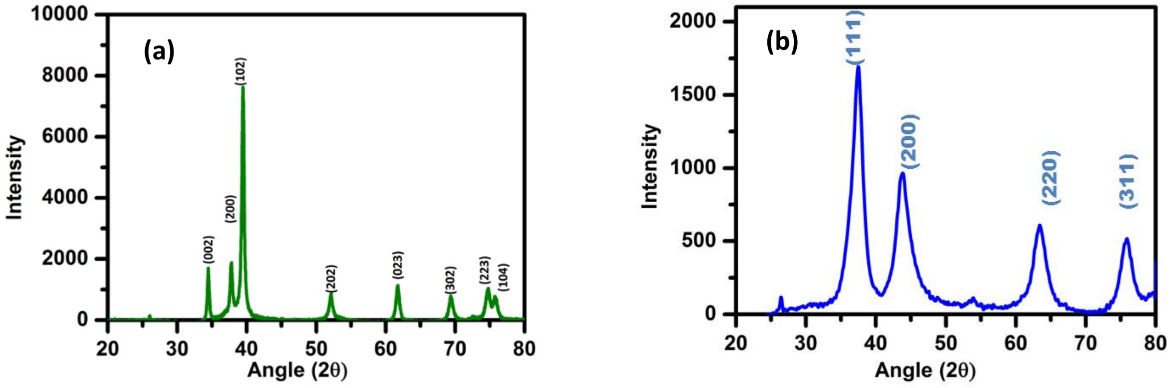

Fig S1.2: PXRD pattern of (a) Mo_2C and (b) Mo_2N

S.2.Electrochemical measurements

S.2.1. General methodology and electrode fabrication

The working electrode was prepared as follows: 4 mg of carbon supported catalyst was dispersed in 495 µl of dimethyformamide and 5 µl of nafion using Labsonic LBS2-10 BATH Sonicator for 60 min. 10 µl of dispersed ink was drop casted on the clean and polished glassy carbon electrode. The electrode was dried under vacuum. Catalytic activity was measured using electrochemical workstation CHI660E. Saturated calomel electrode, carbon electrode and glassy carbon electrode were used as reference, counter and working electrode respectively. Polarization curves were collected in a Ar purged 1 M H_2SO_4 solution at scan rate of 2 mV s $^{-1}$ The long-term durability tests were performed in an Ar-purged 1 M H_2SO_4 solution by recording the overpotential needed to drive 10 mA cm^{-2} of current density. The overpotential of all catalytic material was quoted with respect to R.H.E electrode and further corrected by ohmic drop according to the equation $\eta_{corrected} = \eta - iR_s$ whereas R_s is solution resistance . The EIS measurements were carried out from 100 000 Hz to 1 Hz at selected values of the overpotential i.e. (η =100, 250 and 400 mV).

S.2.2. Stability curve of molybdenum carbide and nitride catalysts

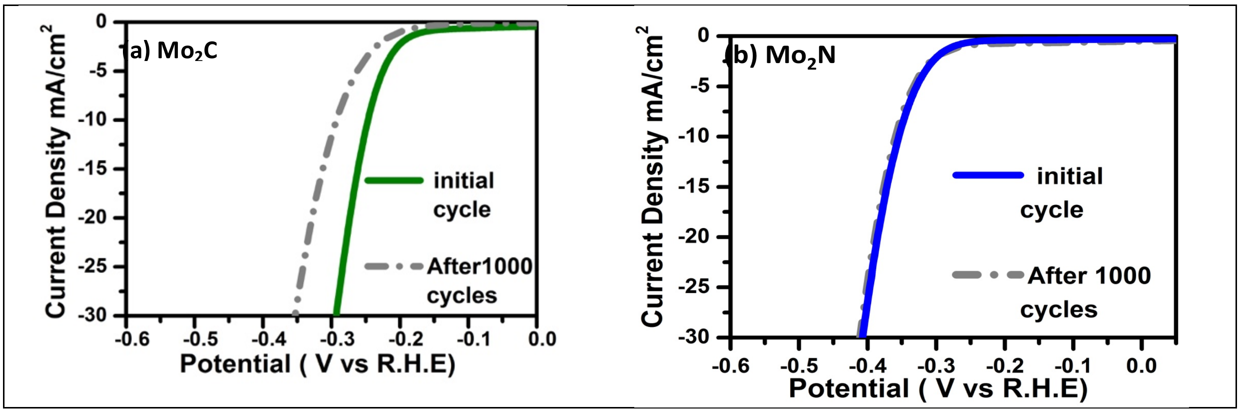

Fig S.2.2: Polarization Curve of (a) Mo_2C (b) Mo_2N before and after 1000 cycle recorded in 1 M H_2SO_4 at scan rate of 7 mV/sec.

S.2.3. EIS measurement of MoCat and MoCat-m catalyst

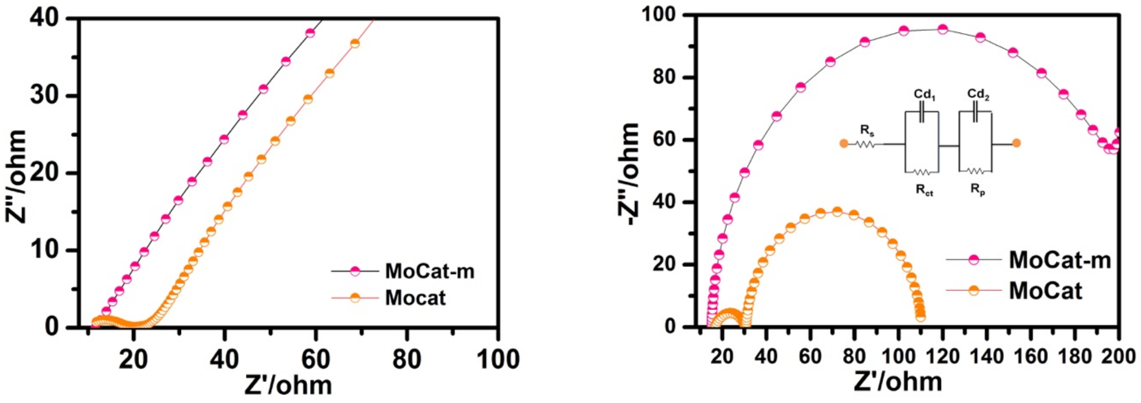

Fig S2.3: (a) Nyquist plot of MoCat and MoCat-m (b) Nyquist plot of MoCat and MoCat-m at 100 mV fitted using RC shown in inset.

S.2.4. Table of comparison of activities of some reported non precious HER catalysts

HER catalysts	Catalyst Loading(mg/cm^2)	η_{10} (mV)	Tafel slope(mV/dec)	Exchange Current Density (mA/cm^2)	References
MoCat catalyst	0.4	96	37	1.8 x 10^{-2}	This work
MoCat-m	0.4	310	61	1.4 x 10^{-3}	This work
MoCx nano-octahedrons	0.8	142	53	0.023	Hao Bin Wu et al. Nat. Commun. 6:6512
α –Mo_2C	0.102	198	56	Not mentioned	Liang Ma et al. J. Mater. Chem. A, 2015, 3,8361
γ-Mo_2N	0.102	381	100	Not mentioned	Liang Ma et al. J. Mater. Chem. A, 2015, 3,8361
Mo_2C/CNT	2.0	152	55.2	1.4 X 10^{-2}	W.-F. Chen et al. J. Mater. Chem. A, 2015, 3,8361
Mo_2C/XC	2.0	~220	59.4	8.1x10^{-3}	W.-F. Chen et al. J. Mater. Chem. A, 2015, 3,8361
Mo2C@NPC/NPRGO15	0.14	34	30	1.09	Ji-Sen Li et al. Nat. Commun. 7:11204
Co-Mo_2C-0.020	0.14	140	39	5.1 X 10^{-3}	Huanlei Lin et al. Adv. Funct. Mater.2016, 26, 5590–5598

S.3. Composition Analysis

S.3.1. Powder X Ray diffraction

Measurements were done with Bruker Eco D8 advance X Ray Powder Diffractometer using Ni filtered with Cu Kα radiation (λ=1.54056 °A). The data were collected from $10^{\circ} < 2\theta < 80^{\circ}$ with increment of 0.019˚.

S.3.2. Rietveld Analysis

Rietveld refinement was carried out using TOPAS 5 software, Bruker.

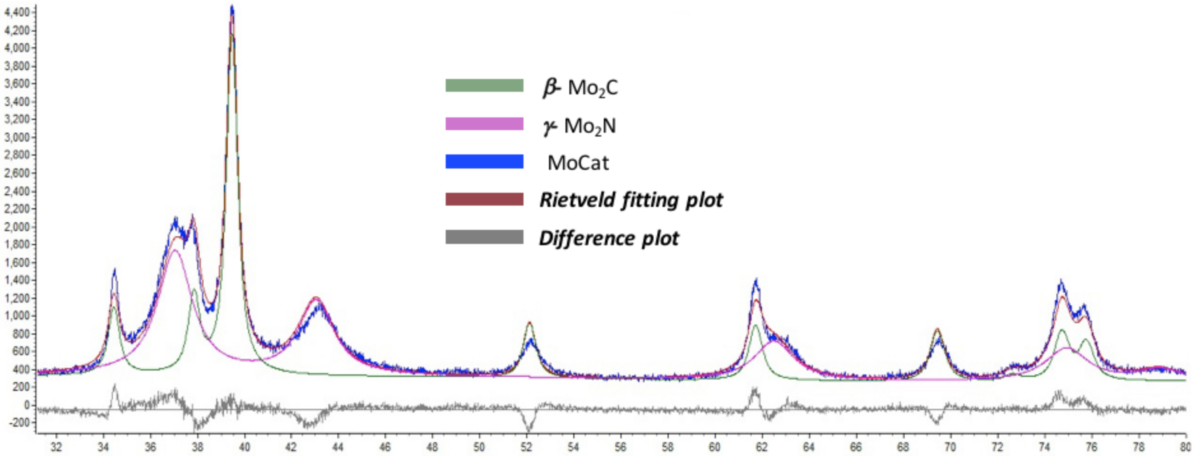

S.3.3. **Electron microscopy**

Morphology studies was done using Scanning electron microscopy with JEOL 7600F FESEM equipped with energy dispersive X-ray diffractometer and Transmission electron microscopy using JEM -2100 TEM operated at 200 kV .

S.3.4. X-ray absorption spectroscopy

EXAFS and XANES measurements have been carried out on the samples Mo_2C, Mo_2N, Mo foil, AMH, MoCat at Mo-K edge.

S.3.4.1. Characterisation of Mo based catalysts by X-ray Absorption Spectroscopy

The **X-ray Absorption Spectroscopy** measurements of the Mo based catalysts along with the Mo standards were carried out at the Energy Scanning EXAFS beamline (BL-9) at the INDUS-2 Synchrotron Source (2.5 GeV, 100 mA), Raja Ramanna Centre for Advanced Technology (RRCAT), Indore, India [3, 4]**.** The beamline uses a double crystal monochromator (DCM) which works in the photon energy range of 4-25 KeV with a resolution of 10^4 at 10 KeV. A 1.5 m horizontal pre-mirror with meridonial cylindrical curvature is used prior to the DCM for collimation of the beam and higher harmonic rejection. The second crystal of the DCM is a sagittal cylindrical crystal, which is used for horizontal focusing of the beam while another Rh/Pt coated bendable post mirror facing down is used for vertical focusing of the beam at the sample position. EXAFS measurements of these samples have been carried out in transmission mode at the Mo K-edge. For measurements in the transmission mode, the sample is placed between two ionization chamber detectors. The first ionization chamber measures the incident flux (I_0) and the second ionization chamber measures the transmitted intensity (I_t) and the absorbance of the sample is obtained as ($\mu = \exp(-\frac{I_t}{I_0})$). The EXAFS spectra of the samples at Mo K-edge were recorded in the energy range 19925-20730eV.

EXAFS: Figure. 2d in the manuscript represents the experimental EXAFS ($\mu(E)$ versus E) spectra of Mo based catalysts samples along with Mo standards at Mo K-edge. In order to take care of the oscillations in the absorption spectra, the energy dependent absorption coefficient $\mu(E)$ has been converted to absorption function $\chi(E)$ defined as follows[5, 6]:

$$\chi(E) = \frac{\mu(E) - \mu_0(E)}{\Delta\mu_0(E_0)} \qquad (1)$$

where E_0 is the absorption edge energy, $\mu_0(E_0)$ is the bare atom background and $\Delta\mu_0(E_0)$ is the step in the $\mu(E)$ value at the absorption edge. After converting the energy scale to the photoelectron wave number scale (k) as defined by,

$$k = \sqrt{\frac{2m(E - E_0)}{{}^{2}}} \qquad (2)$$

the energy dependent absorption coefficient $\chi(E)$ has been converted to the wave number dependent absorption coefficient $\chi(k)$, where m is the electron mass. Finally, $\chi(k)$ is weighted by k to amplify the oscillations at high k and the $\chi(k)\,k$ functions are Fourier transformed in R space to generate the $\chi(R)$ versus R (or FT-EXAFS) spectra in terms of the real distances from the center of the absorbing atom. It should be mentioned here that a set of EXAFS data analysis program available within the IFEFFIT software package have been used for reduction and fitting of the experimental EXAFS data[7]. This includes data reduction and Fourier transform to derive the $\chi(R)$ versus R spectra from the absorption spectra (using ATHENA software), generation of the theoretical EXAFS spectra starting from an assumed crystallographic structure and finally fitting of the experimental data with the theoretical spectra using the FEFF 6.0 code(using ARTEMIS software). The bond distances (R), co-ordination numbers (including scattering amplitudes) (CN) and disorder (Debye-Waller) factors (σ^2), which give the mean-square fluctuations in the distances, have been used as fitting parameters. The goodness of the fit in the above process is generally expressed by the R_{factor} which is defined as:

$$R_{factor} = \sum \frac{[\mathrm{Im}(\chi_{dat}(r_i) - \chi_{th}(r_i)]^2 + [\mathrm{Re}(\chi_{dat}(r_i) - \chi_{th}(r_i)]^2}{[\mathrm{Im}(\chi_{dat}(r_i)]^2 + [\mathrm{Re}(\chi_{dat}(r_i)]^2} \qquad (3)$$

where, χ_{dat} and χ_{th} refer to the experimental and theoretical $\chi(r)$ values respectively and Im and Rerefer to the imaginary and real parts of the respective quantities. Figure 3 shows the Fourier transformed EXAFS (FT-EXAFS) $\chi(R)$ versus R spectra of all the Mo based catalyst samples at the Mo K-edge along with the best fit theoretical spectra. The data has been fitted in the k range of 3-10 Å^{-1} and upto 3.6 Å in R space. Best fit parameters of Mo_2N and Mo_2C and MoCat are shown in Table-T1 & Table-T2.

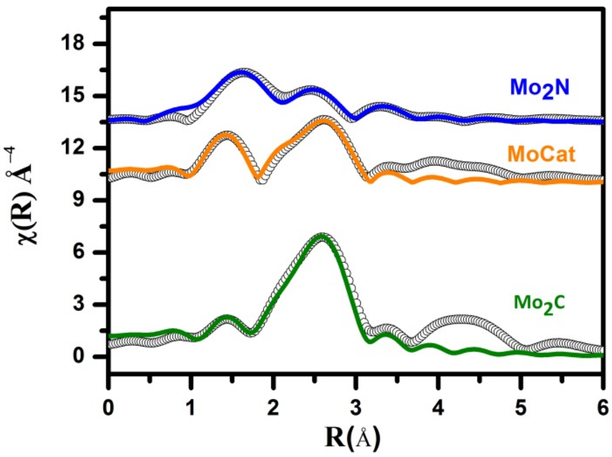

Fig. S3: The experimental $\chi(R)$ versus R spectra and the theoretical fits of Mo based catalyst samples at Mo K-edge.

Table: T1

(Mo$_2$N structure)		Mo$_2$N
Mo-N	CN(6)	4.72±0.96
	R	2.08±0.02
	σ^2	0.016±0.002
Mo-Mo	CN(12)	10.82±2.04
	R	2.86±0.02
	σ^2	0.018±0.001
Mo-N	CN(8)	8.96±1.36
	R	3.62±0.02
	σ^2	0.002±0.001
R_{factor}		0.004

Table: T2

		Mo$_2$C	MoCat
Mo-C	CN(6)	5.53±1.26	5.53±1.26
	R	2.14±0.04	2.17±0.02
	σ^2	0.024±0.009	0.014±0.003
Mo-Mo	CN(12)	11.46±1.68	10.8±2.28
	R	2.93±0.01	2.94±0.01
	σ^2	0.011±0.001	0.014±0.001
R_{factor}		0.001	0.005

ESI 4: BET analysis in details.

BET analysis was done in Autosorb IQ Qunatchrome instrument. The surface area of MoCat catalyst comes out be $254 m^2/g$ having average pore size between 1-2 nm.

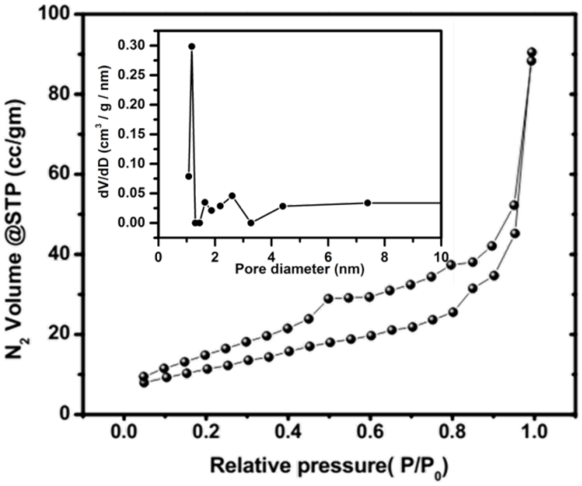

Fig S4: BET isotherm of MoCat catalyst with BJH pore size distribution shown in inset

ESI 5: Theoretical Section

S. 5.1. Computational details

All the calculation has been performed using density functional theory within the frame of Vienna ab-initio simulation package (VASP).[8-11] All the energies have been calculated self-consistently with generalized gradient approximation (GGA) using Perdew-Burke-Ernzerhof exchange correlation functional.[12, 13] The electron ion interaction is described by projector-augmented plane wave (PAW).[14, 15] Convergence threshold for energy and force are set at 10^{-4} eV and 0.03 eV/Å.

Theoretical models

For the comparative, we have constructed the theoretical model of slabs of Mo_2C, Mo_2N, and interface of Mo_2C-Mo_2N, H @ Mo_2C, H @Mo_2N and H@Mo_2C-Mo_2N. Particularly we have considered 001 facet with Mo-terminated surface as an active surface of β-phase of Mo_2C and ɣ-phase of Mo_2N. Nanoparticles of Mo_2C and Mo_2N are constructed by modelling the slab with six layers of Mo-C and four layers of Mo-N. All the geometries are relaxed using selective dynamics implemented within VASP by keeping first three layers translate and rest layers fix. Different adsorption sites have been considered for the H atoms over Mo_2C, Mo_2N and Mo_2C-Mo_2N (as shown in Fig S.5.1). In case of Mo_2C, hydrogen is adsorbed over the center. In Mo_2N, H is adsorbed over the center, over the Mo atom and over the N atom. In case of interface Mo_2C and Mo_2N two adsorption sites have been considered: one is over the Mo side and another is over the N-atom near the interface.

Initial geometries of Mo_2C, Mo_2N and Mo_2C-Mo_2N are depicted in Fig S.5.1

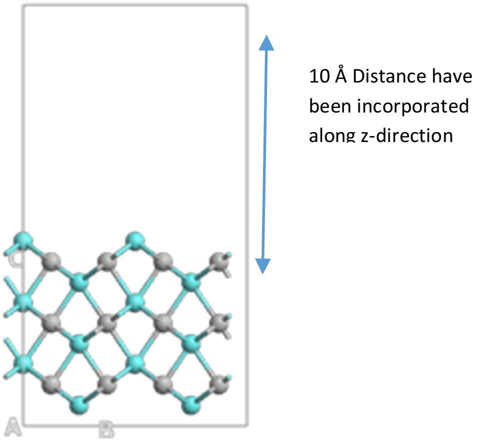

10 Å Distance have been incorporated along z-direction

Mo_2C

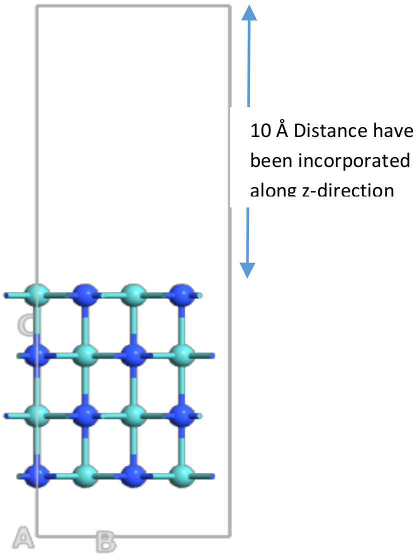

10 Å Distance have been incorporated along z-direction

Mo_2N

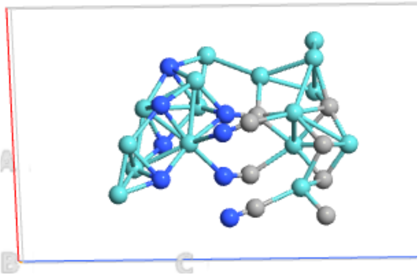

Mo_2C-Mo_2N

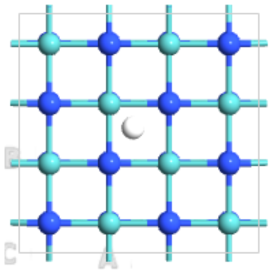

H@Mo_2N
(Top view)
Adsorption over the centre
(d)

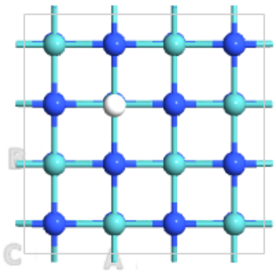

H@Mo_2N
(Top view)
Adsorption over the Mo
(d)

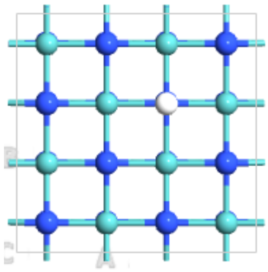

H@Mo_2N
(Top view)
Adsorption over the Mo
(d)

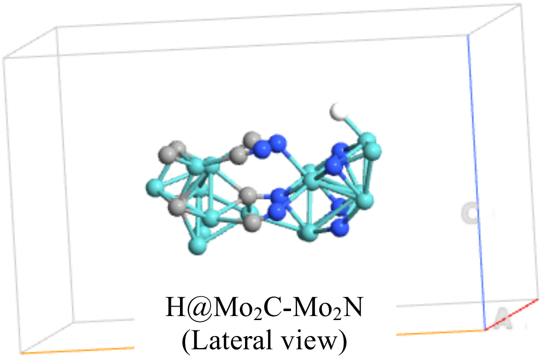

H@Mo_2C-Mo_2N
(Lateral view)
Adsorption over Mo atom
(d)

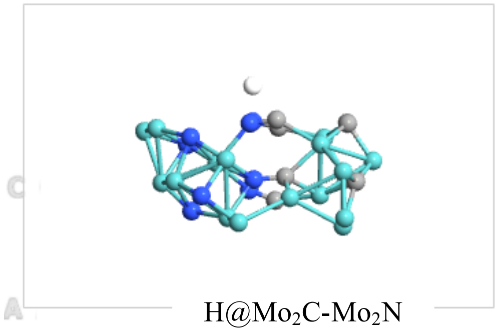

H@Mo_2C-Mo_2N
(Lateral view)
Adsorption over the interface
(d)

Fig S.5.1: Initial geometries of pristine and adsorbed system of Mo_2C, Mo_2N and Mo_2C-Mo_2N Relaxed geometries of pristine and hydrogen adsorbed over the nanoparticles Mo_2C, Mo_2N, and Mo_2C-Mo_2N are shown in Fig S.5.2.

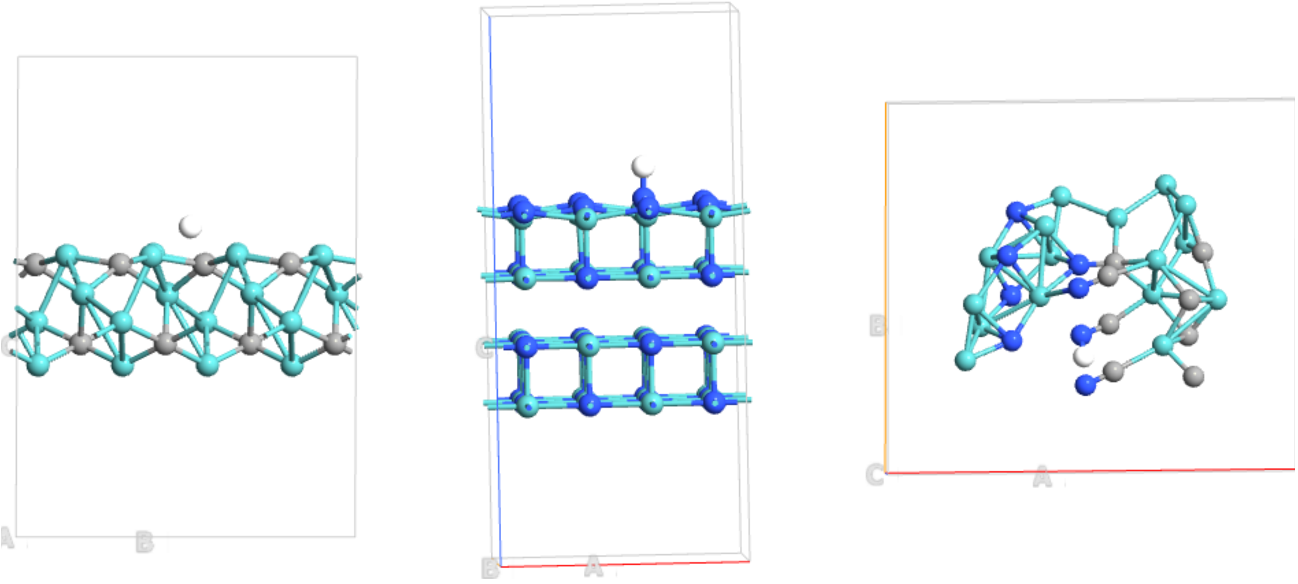

H@Mo_2C (Lateral view)
(a)

H@Mo_2N
(Lateral view)
(b)

H@Mo_2C-Mo_2N
(Lateral view)

Fig S.5.2 Relaxed geometries of hydrogen adsorption over Mo_2C, Mo_2N and Mo_2C-Mo_2N

S.5.2. Adsorption energy of hydrogen over Mo_2C, Mo_2N and Mo_2C-Mo_2N

Further adsorption energy of hydrogen is computed over the slabs as follows

$$\Delta E_H = E(system + H) - E(system) - E(H)$$

Where E(system+H) is the total energy of system with H atom adsorbed on the surface, E (system) is the total energy of system and E (H) is the total energy of H atom.

Table T3: Adsorption energy and Gibbs free for all the systems

System	Adsorption energy (E_d) (in eV)	Gibbs free energy (ΔG_H) (in eV)
H@Mo_2C	-1.89	-1.65
H@Mo_2N	-2.84	-2.60
H@Mo_2C-Mo_2N	-0.23	0.12

Table T4. The lattice parameters (Å) of the supercells for all the systems.

Table	a	b	c
Mo_2C	9.472	12.116	20
Mo_2N	6.642	6.642	20
Mo_2C-Mo_2N	9.044	15.400	17.77
H@Mo_2C	9.681	11.671	16.571
H@Mo_2N	8.366	8.399	19.106
H@Mo_2C-Mo_2N	15.743	19.915	12.634

Different adsorption site of Mo_2C, Mo_2N and interface $Mo_2C\_Mo_2N$

For the hydrogen adsorption over Mo_2C, Mo_2N, and Mo_2C-Mo_2N, different adsorption sites have been explored in the present study. Herein, we have considered only that site which is most appropriate for the H-adsorption. For example, for the Mo_2N, three adsorption sites have been explored; over the center of the square in the top view of Mo_2N, on top Mo-atom and on top N-atom. The corresponding initial geometry, final geometry, and the respective associated total free energy are displayed below:

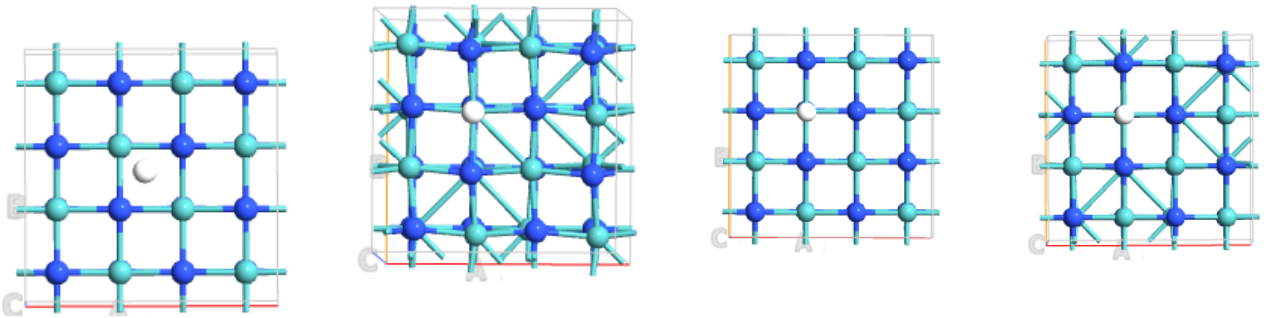

Mo_2N_Centre_H_Initial

Mo_2N_Centre_H_final

E= -620.25 eV

Mo_2N_ontop_Mo

_Initial

Mo_2N_ontop_Mo_final

E= -619.68 eV

Top View

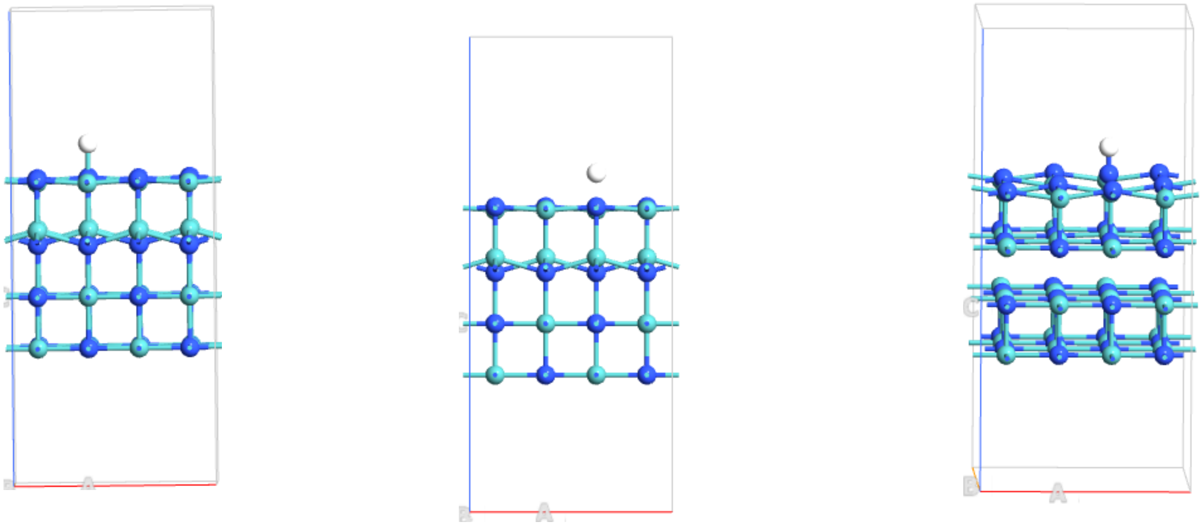

Mo_2N_ontop_Mo_final

E= -619.68 eV

Side View

Mo_2N_ontop_Mo_Initial

Mo_2N_ontop_N_final

E= -626.38 eV

Side View

Figure1: Different adsorption site for the H adsorption over the Mo_2N

From the above figure, it is clear that adsorption site over the N-atom is the lowest energy structure. Therefore, top N is the most appropriate site for the H-adsorption over the Mo_2N. In a similar manner, two adsorption sites have been explored for the Mo_2C slab: between two Mo-atoms and over the bridge of Mo-C. Top view of $Mo_2C$is shown below. From the thorough analysis, we find that position between Mo-atoms would be more appropriate for the H-adsorption.

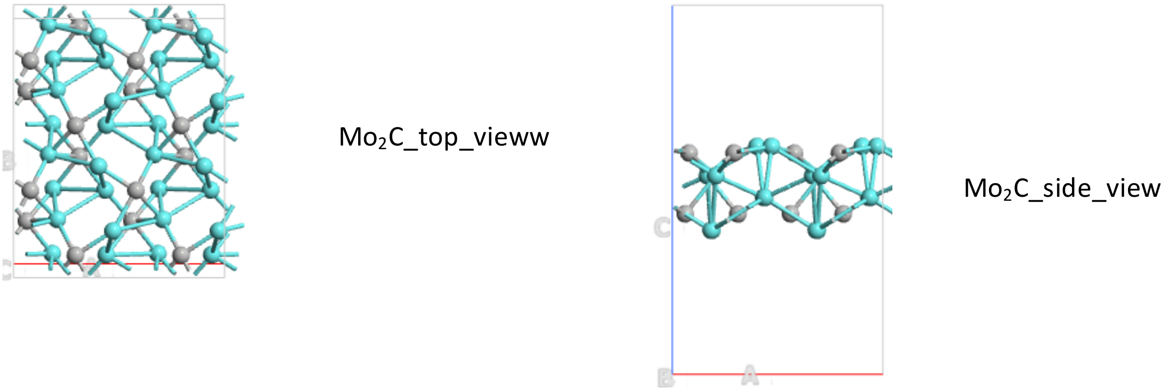

Figure 2: Top and side view of Mo_2C

For the interface of Mo_2C_Mo_2N, particularly, two sites have been checked for the H adsorption: away from the interface (a), near the interface (b) and we find that interfacial region of Mo_2C and Mo_2N is preferable for the adsorption of Hydrogen. This point is well explained in the manuscript in terms of Bader charge distribution analysis.

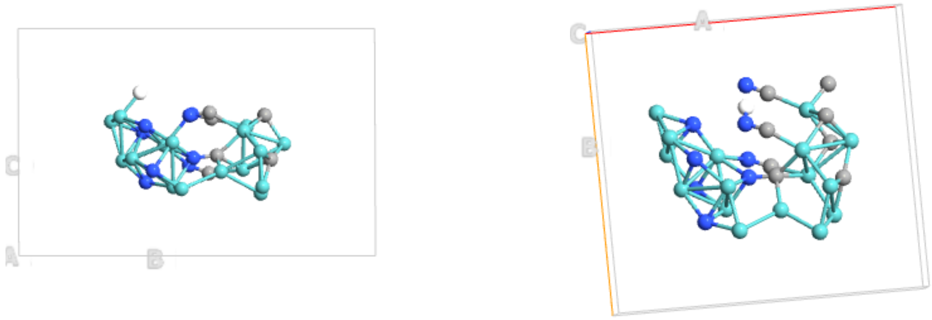

Mo_2C_Mo_2N (a)

Mo_2C Mo_2N (b)

Figure 3: H adsorption away from the interface of Mo_2C_Mo_2N (a), over the Interface of Mo_2C_Mo_2N

References:

1. J. Liu, T. Zhang, Z. Wang, G. Dawson and W. Chen, *Journal of Materials Chemistry*, 2011, **21**, 14398-14401.
2. L. E. Toth, *Journal of the Less Common Metals*, 1967, **13**, 129-131.
3. S. Basu, C. Nayak, A. Yadav, A. Agrawal, A. Poswal, D. Bhattacharyya, S. Jha and N. Sahoo, 2014.
4. A. Poswal, A. Agrawal, A. Yadav, C. Nayak, S. Basu, S. Kane, C. Garg, D. Bhattachryya, S. Jha and N. Sahoo, 2014.
5. S. Kelly, D. Hesterberg and B. Ravel, *Methods of soil analysis. Part*, 2008, **5**, 387-463.
6. D. Koningsberger and R. Prins, 1988.
7. M. Newville, B. Ravel, D. Haskel, J. Rehr, E. Stern and Y. Yacoby, *Physica B: Condensed Matter*, 1995, **208**, 154-156.
8. G. Kresse and J. Hafner, *Physical Review B*, 1994, **49**, 14251.
9. G. Kresse and J. Furthmüller, *Computational Materials Science*, 1996, **6**, 15-50.
10. G. Kresse and J. Hafner, *Physical Review B*, 1993, **47**, 558.
11. G. Kresse and J. Furthmüller, *Physical review B*, 1996, **54**, 11169.
12. J. P. Perdew, K. Burke and M. Ernzerhof, *Physical review letters*, 1996, **77**, 3865.
13. K. Burke, J. P. Perdew and M. Ernzerhof, *Phys. Rev. Lett*, 1997, **78**, 1396.
14. P. E. Blöuml, *Phys Rev B*, 1994, **50**, 17953-17979.
15. G. Kresse and D. Joubert, *Physical Review B*, 1999, **59**, 1758.